

A brief report on statistical study of net electric current in solar active regions with longitudinal fields of opposite polarity *

Y. Gao¹

Key Laboratory of Solar Activity, National Astronomical Observatories, National Astronomical Observatories, Chinese Academy of Sciences, Beijing 100012, China; gy@bao.ac.cn

Received [year] [month] [day]; accepted [year] [month] [day]

Abstract Dynamic processes occurring in solar active regions are dominated by the solar magnetic field. As of now, observations using a solar magnetograph have supplied us with the vector components of a solar photospheric magnetic field. The two transverse components of a photospheric magnetic field allow us to compute the amount of electric current. We found that the electric current in areas with positive (negative) polarity due to the longitudinal magnetic field have both positive and negative signs in an active region, however, the net current is found to be an order-of-magnitude less than the mean absolute magnitude and has a preferred sign. In particular, we have statistically found that there is a systematic net electric current from areas with negative (positive) polarity to areas with positive (negative) polarity in solar active regions in the northern (southern) hemisphere, but during the solar minimum this tendency is reversed over time at some latitudes. The result indicates that there is weak net electric current in areas of solar active regions with opposite polarity, thus providing further details about the hemispheric helicity rule found in a series of previous studies.

Key words: Sun: activity — Sun: photosphere — Sun: magnetic fields

1 INTRODUCTION

In the solar atmosphere, a chirality has been found in the photospheric magnetic field of active regions that is usually described by the parameter of current helicity or force-free field factor. In the northern (southern) solar hemisphere, the helicity mainly possess left (right) handedness, and is called the hemispheric helicity sign rule (Seehafer 1990; Pevtsov et al. 1994; Pevtsov et al. 1995; Abramenko et al. 1996; Bao & Zhang 1998; Hagino & Sakurai 2004; Zhang et al. 2010). Furthermore, the distribution of helicity signs was investigated between the 23rd and 24th solar activity cycles (e.g., Hao & Zhang 2011). Generally, both left and right handed chirality coexist on a particular pixel in an image of solar active region, or even a sunspot, used in deriving a solar vector magnetogram. The physical explanation of the hemispheric helicity sign rule is still a complicated problem. Some typical case studies have shown that there are systems with opposite net current in several active regions (Wang et al. 1994; Leka et al. 1996; Wang & Abramenko 1999; Wheatland, 2000). However, it was also inferred that there was no net current in sunspots (Venkatakrishnan & Tiwari 2009). The application of the parameter describing current helicity in active regions has again come into question. In this paper, we try separating the positive and negative flux areas according to the longitudinal field of the solar active region and study the distribution of current. In Section 2, we describe the procedure of observation for this analysis, and present data reduction and result in Section 3. We then summarize and discuss our results in Section 4.

* Supported by the National Natural Science Foundation of China.

2 OBSERVATIONS

Vector magnetograms were observed using the Solar Magnetic Field Telescope (SMFT), which has a tunable birefringent filter-type video vector magnetograph (Ai 1987). For photospheric observations, the passband of the filter is set at FeI $\lambda 5324 \text{ \AA}$. Normally the longitudinal component of the field (Stokes V) is measured at -75 m\AA and the transverse components (Stokes Q and U) are measured at the line core. The equivalent width of the FeI $\lambda 5324 \text{ \AA}$ line is 0.344 \AA and the FWHM of the filter passband is 0.15 \AA . Vector magnetograms are reconstructed by the following relations:

$$B_{\parallel} = C_{\parallel} \frac{V}{I} \quad (1)$$

$$B_{\perp} = C_{\perp} \left[\left(\frac{Q^2}{I} + \frac{U^2}{I} \right) \right]^{1/4} \quad (2)$$

in which C_{\parallel} and C_{\perp} are the calibration coefficients for the longitudinal and transverse fields (Su & Zhang 2004). The azimuthal angle of the transverse field is

$$\phi = \frac{1}{2} \arctan \left(\frac{U}{Q} \right) \quad (3)$$

Thus the y - and x - components of the vector magnetic field are as follows:

$$B_y = B_{\perp} \sin \phi \quad (4)$$

$$B_x = B_{\perp} \cos \phi \quad (5)$$

The 180° ambiguity in the direction of the transverse field is resolved following Wang et al. (1994) by comparison with the potential field. The active regions under investigation are all located near the center of the disk. The latitude and longitude are less than 40° , so that the projection effects are small. Therefore we may denote the line-of-sight and horizontal components of magnetic field as B_z and B_t , respectively. Usually, in our computations, we select the pixels where the signal exceeds the noise levels $|B_z| > 20G$ and $B_t > 100G$. The difference in the method used for data reduction compared with previous research is that we compute the average value of J_z ($\langle J_z \rangle$) on the pixels where ($B_z > 20G$, $B_t > 100G$) or ($B_z < -20G$, $B_t > 100G$) respectively. The derived parameter is longitudinal electric current, which is defined as $J_z = (1/\mu_0)(\partial B_y/\partial x - \partial B_x/\partial y)$.

3 DATA REDUCTION

3.1 Case of NOAA 10484

Figure 1 shows a simple relation between the electric current and positions of the pixels. The top panel shows the electric current in areas with both positive and negative longitudinal fields in the active region NOAA 10484. The middle and bottom panels show the electric current in areas with only positive or negative longitudinal field respectively. Compared with the top panel, the bottom two show a weak negative and positive deviation in electric current respectively, in spite of all their standard deviations being of the same order.

Figure 2 shows the detailed information on the distribution of the electric current of NOAA 10484. The vector magnetogram was observed at 09:49:42 on 2003 Oct 22. There are three columns in Figure 2, the first column shows the distribution of electric current in areas with both positive and negative longitudinal fields. The color patterns in row 2 - 4 show the J_z in intervals with an order-of-magnitude $< 10^0$ to 10^{-4} respectively. The number of pixels where $|J_z| > 10^0 \text{ A}$ accounts for 2.5% of the total. The number of pixels where $|J_z| < 10^{-3} \text{ A}$ accounts for 57% of the total, but the $\langle |J_z| \rangle$ is only on the order of 10^{-5} , which is not shown in this figure. The main contribution of $\langle |J_z| \rangle$ has an order-of-magnitude of $10^{-3} - 10^0 \text{ A}$, as shown in the Row 2-4 of the first column.

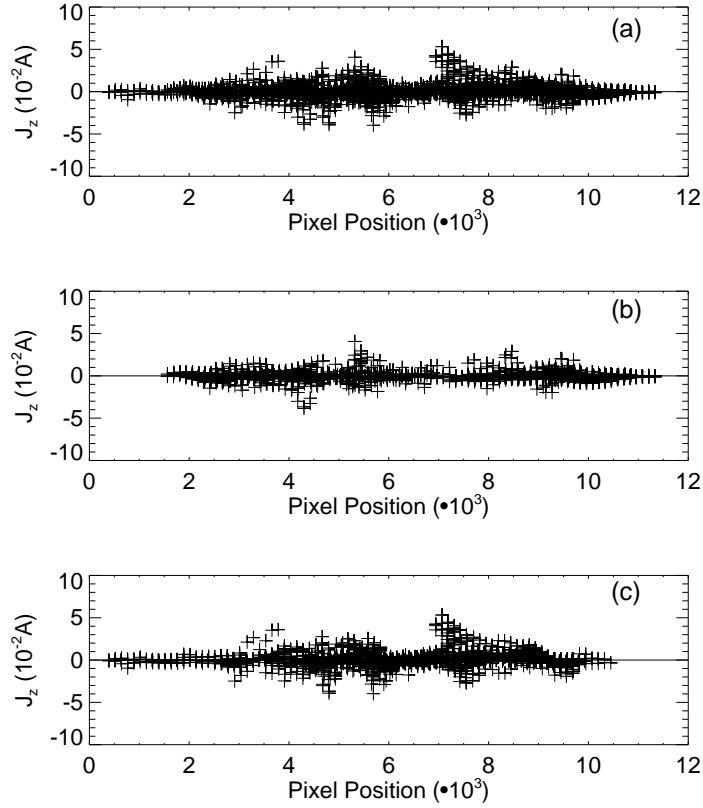


Fig. 1 Electric current as a function of pixel position. (a) shows the electric current with both positive and negative longitudinal fields in the active region NOAA 10484. The average and standard deviation are 1.0×10^{-2} A and 6.6×10^{-1} A, respectively. (b) shows the electric current in areas with only positive longitudinal fields. The average and standard deviation are -7.6×10^{-2} A and 5.0×10^{-1} A, respectively. (c) shows the electric current in areas with only negative longitudinal fields. The average and standard deviation are 7.4×10^{-2} A and 7.5×10^{-1} A, respectively.

The second column shows the distribution in areas with only a positive longitudinal field. It is found that a mean current -1.61×10^{-2} , -1.68×10^{-2} and -2.96×10^{-4} A with a magnitude smaller than the mean absolute magnitude of 5.13×10^{-2} , 4.46×10^{-2} and 3.05×10^{-3} A corresponding to the orders of 10^0 , 10^{-1} and 10^{-2} A, respectively.

The third column shows the distribution in areas with only a negative longitudinal field. It is found that there is a mean current of 1.69×10^{-2} , 3.43×10^{-3} and -4.95×10^{-4} A with a magnitude smaller than the mean absolute magnitude of 9.74×10^{-2} , 6.34×10^{-2} and 3.36×10^{-3} A corresponding to the order of 10^0 , 10^{-1} and 10^{-2} , respectively.

3.2 Statistic Study of Large Sample

We analyze a database of 6629 vector magnetograms observed at Huairou Solar Observing Station from 1988 to 2005. For more detailed information, the reader is referred to Zhang et al. (2010). The effective field of view is $5.23' \times 3.63'$ (before 2001 Aug 25), $4.06' \times 2.77'$ (2001 Aug 25 to 2001 Oct 13 and 2001

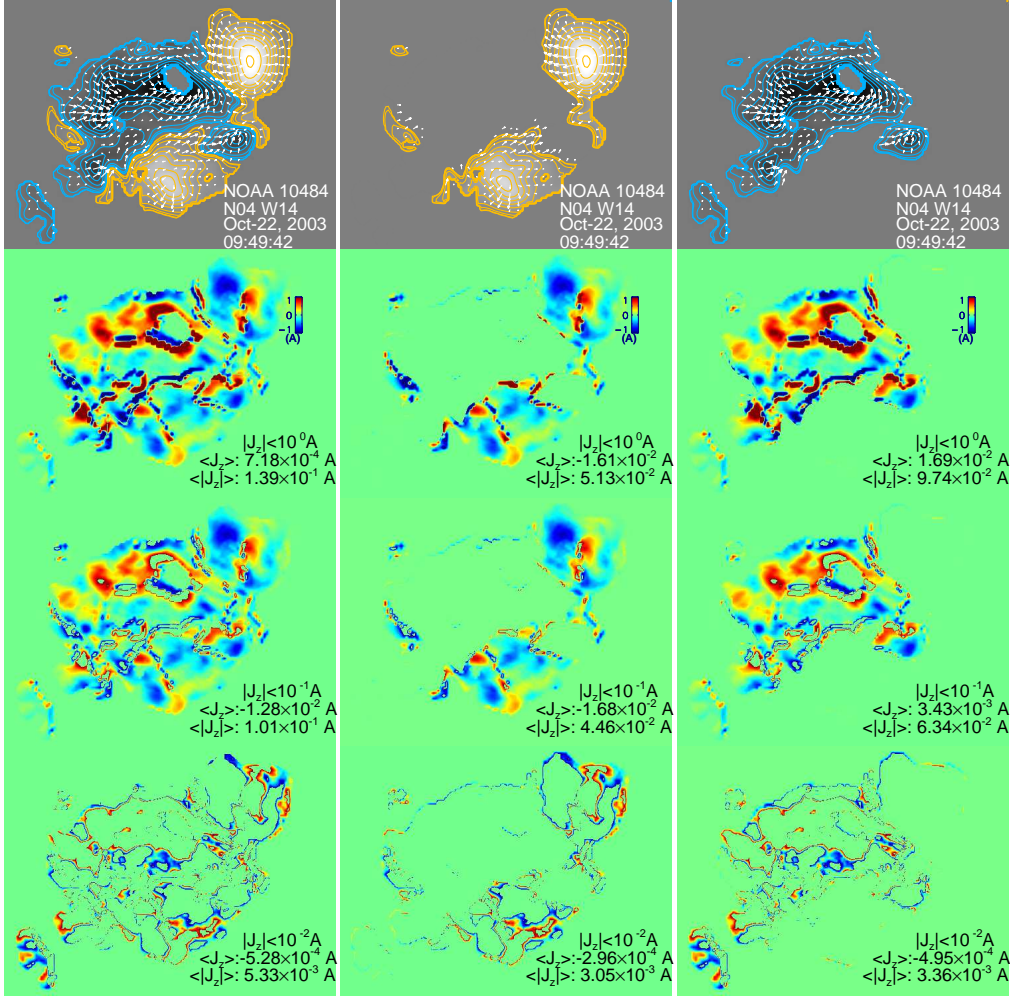


Fig. 2 The top panels in each column show the original vector magnetogram and the gray-scale images show the longitudinal magnetic field of NOAA 10484. The orange (cyan) contours show the positive (negative) longitudinal magnetic field. The contour levels are [30, 160, 480, 800, 1280, 1600G]. The first column shows the distribution of electric current in areas with both positive and negative longitudinal fields. The second column shows the distribution in the area with only a positive longitudinal field. The third column shows the distribution in the area with only a negative longitudinal field. The images from the second to fourth rows show the electric current. The corresponding scale of magnitude is shown in the bottom right corner of each plot.

Oct-14 to Nov-30) and $3.75' \times 2.81'$ (after 2001 Dec 1). After obtaining $\langle J_z \rangle$ for each magnetogram, we compute the 2-year running average value in a 7° range of latitudes. Then we derive butterfly diagrams, as shown in the figure 3.

Figure 3 shows that the $\langle J_z \rangle$ is negative (positive) in areas with positive (negative) magnetic polarity in northern hemisphere or positive (negative) in areas with positive (negative) magnetic polarity in the southern hemisphere in most bins. The colored background is the butterfly diagram of sunspot areas. The vertical colored bar beside the upper (lower) panel indicates that the leading polarity is mainly negative

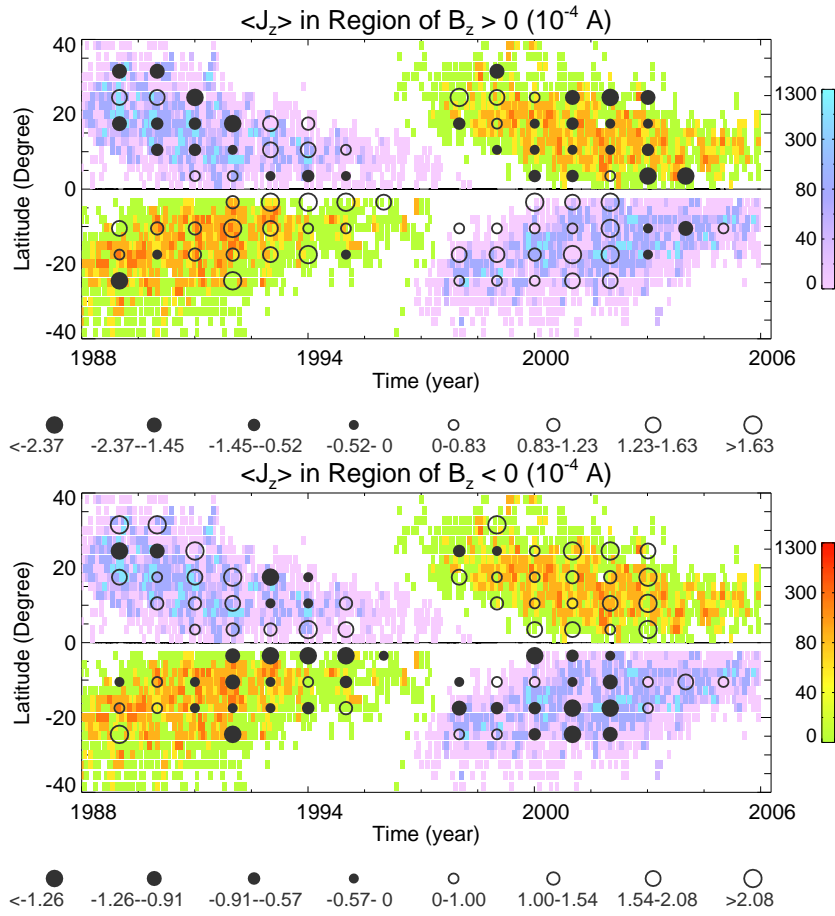


Fig. 3 The solid circles (*filled circles*) show the positive (negative) sign of the mean electric current. The sizes of the circles are proportional to the magnitude of the displayed quantity. The underlying colored “butterfly diagram shows how sunspot density varies with latitude over the solar cycle. The upper (lower) vertical color bar on the right represents the leading sunspot having negative (positive) polarity.

(positive) and the following polarity is mainly positive (negative). So the whole butterfly diagram statistically indicates that the direction of the weak net current points from sunspots with negative (positive) polarity to ones with positive (negative) polarity in the northern (southern) hemisphere. Additionally, there are obvious exceptions at the minimum of the solar activity cycle. This implies that a statistical reversal in the sign of helicity at the minimum of the solar activity cycle is an intrinsic property of evolution of the solar magnetic field. It should be pointed out that exceptions are found not only in the minimum but also in the whole solar activity cycle. The percentage of exceptions is relatively higher at the minimum than in other phases of the solar cycle.

Figure 4 shows two exceptions. The upper panels show a vector magnetogram of NOAA 9690 (left) where the distribution of electric current by order-of-magnitude is less than 10^0 A (right). The $\langle J_z \rangle$ is $-1.22 \times 10^{-2} A$ compared to the $\langle |J_z| \rangle$ of $1.08 \times 10^{-1} A$ (11.3%). The bottom panels show the vector magnetogram of NOAA 8675 (Left) and the distribution of electric current by order-of-magnitude is less than $10^0 A$ (right). The $\langle J_z \rangle$ is $-2.06 \times 10^{-3} A$ compared to the $\langle |J_z| \rangle$ of $1.86 \times 10^{-2} A$ (11.1%).

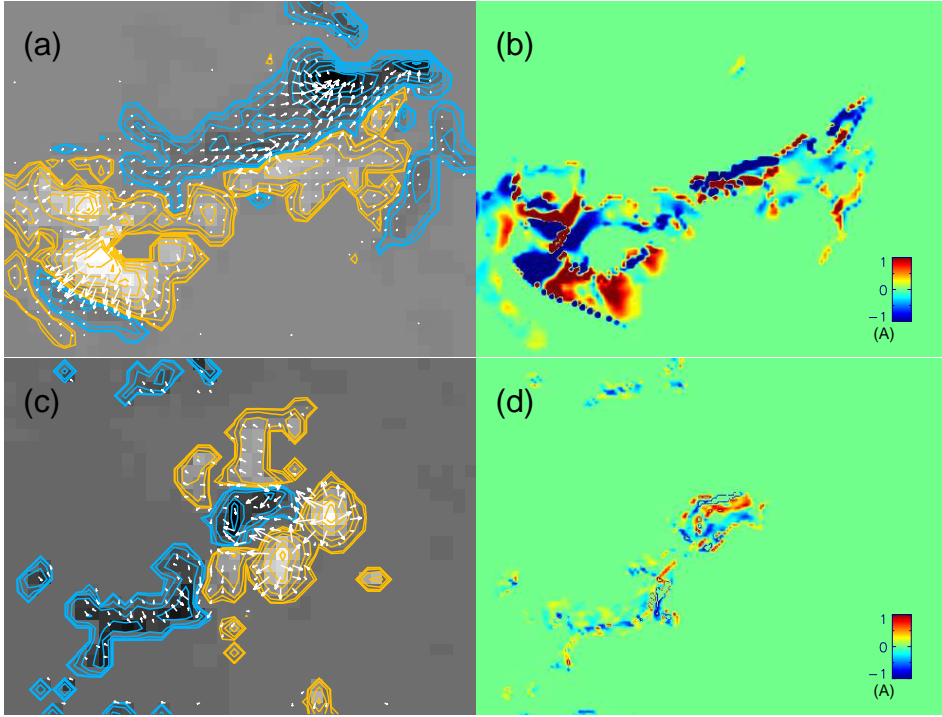


Fig. 4 (a) The upper panels show a vector magnetogram of NOAA 9690 which was located at S17E31 and observed at 11:38:58 on 2001 Nov 08 and (b) areas where the distribution of electric current is in an area with positive polarity. (c) The bottom panels show a vector magnetogram of NOAA 8657 which was located at N19W12 and observed at 02:50:01 on 1999 Aug 31 and (d) areas where the distribution of electric current is in an area with negative polarity.

4 CONCLUSIONS AND DISCUSSION

Through analyzing magnetograms, we have statistically found that there is a systematic net electric current from areas with negative (positive) polarity to areas with positive (negative) polarity in solar active regions in the northern (southern) hemisphere. The tiny net electric current ($\langle J_z \rangle$) is an order-of-magnitude smaller than the mean absolute magnitude of electric current $\langle |J_z| \rangle$ in the whole active region. This current reveals more details about the hemispheric helicity sign rule found in a series of previous studies. For example, the net current is statistically negative in areas with positive (negative) polarity for solar active regions in the northern (southern) hemisphere. As a result, this will cause an excess negative (positive) current helicity in the northern (southern) hemisphere, which is consistent with the sign preference associated with the hemispheric helicity sign rule.

At the minimum in the solar activity cycle, some exceptions of net electric current have been found, which have an opposite direction with respect to the normal ones. This gives self-consistent evidence that the reversal sign of helicity based on observations from the Huairou Solar Observing Station reflects the intrinsic property of twist in the solar magnetic field. Furthermore, we compute the percent of active regions conforming or not conforming to the hemispheric helicity sign rule.

As given in Table 1, bold text shows the cases that follow the overall pattern. Besides a weak preference in sign, there are some unusual features. For the 22nd solar cycle, the percentages are 67.6% (61.9%) when $B_z > 0$ ($B_z < 0$) in the southern (northern) hemisphere. The percentages are higher

Hemisphere	$\langle J_z \rangle > 0, B_z > 0$	$\langle J_z \rangle < 0, B_z > 0$	$\langle J_z \rangle > 0, B_z < 0$	$\langle J_z \rangle < 0, B_z < 0$
22 nd cycle				
North	53.6%	46.3%	61.9%	38.1%
South	67.6%	32.4%	48.4%	51.6%
23 rd cycle				
North	48.9%	51.1%	67.8%	32.3%
South	62.7%	37.3%	46.9%	53.1%

Table 1 The percentages of active regions following (bold text) or not following to the pattern of hemispheric helicity sign rule.

than 51.6% (46.3%) when $B_z < 0$ ($B_z > 0$) in the southern (northern) hemisphere. For the 23rd solar cycle, the percentages are 62.7% (67.8%) when $B_z > 0$ ($B_z < 0$) in the southern (northern) hemisphere. The percentages are still higher than 51.1% (53.1%) when $B_z < 0$ ($B_z > 0$) in the southern (northern) hemisphere. This imbalance of net current in different hemispheres when $B_z < 0$ or $B_z > 0$ may arise from the effect of Faraday rotation, which can cause an excess in false net positive current in an active region (Hagino and Sakurai, 2004; Gao et al., 2008). Nevertheless, the areas with negative current in the southern (northern) hemisphere of $B_z > 0$ ($B_z < 0$) show convincing features that support the reversal in the sign helicity being independent of the effect of Faraday rotation. Although the hemispheric helicity sign rule holds over the whole 23rd solar activity cycle, the apparent areas of reversal sign are seen in the southern hemisphere at the end of the cycle. This is in agreement with another statistical analysis done by Hao and Zhang (2011) with independent data observed by Hinode in the descending phase of 23rd solar activity cycle.

Acknowledgements I am grateful to the referee for helpful comments and suggestions. The work is supported by the National Natural Science Foundation of China (Grant Nos. 11273034, 11178005, 41174153, 11173033, 11103037), the National Basic Research Program of China (973 program, 2011CB811401), and Chinese Academy of Sciences under Grant KJ CX2-EW-T07.

References

- Abramenko, V. I., Wang, T. J. & Yurchishin, V. B. 1996, *Solar Phys.*, 168, 75
 Ai, G. 1987, Publ. Beijing Astron. Obs., No 9, 27-36
 Bao, S. D. & Zhang, H. Q. 1998, *ApJ*, 496, L43.
 Gao, Y., Su, J.; Xu, H. & Zhang, H. 2008, *MNRAS.*, 386., 1959G.
 Hagino, M. & Sakurai, T. 2004, *PASJ*, 56, 831.
 Hao, J. & Zhang, M. 2011, *ApJ*, 733, L27.
 Leka, K. D., Canfield, R. C., McClymont, A. N. & van Driel-Gesztelyi, L. 1996, *ApJ*, 462, 547.
 Pevtsov, A. A., Canfield, R. C. & Metcalf, T. R. 1994, *ApJ*, 425, L117.
 Pevtsov, A. A., Canfield, R. C. & Metcalf, T. R. 1995, *ApJ*, 440, L109.
 Seehafer, N. 1990, *Solar Phys.*, 125, 219.
 Su, J. T. & Zhang, H. 2004, *Chinese Astronomy and Astrophysics*, 4, 365;
 Venkatakrisnan, P. & Tiwari, S. K. 2009, *ApJ*, 706, L114.
 Wheatland, M. S. 2000, *ApJ*, 532, 616.
 Wang, T. J., Xu, A. A. & Zhang H. Q. 1994, *Solar Phys.*, 155, 99.
 Wang, T. J. & Abramenko, V. A. 1999, *ESASP*, 448, 671.
 Zhang, H. Q., Sakurai, T., Pevtsov, A., Gao, Y., Xu, H. Q., Sokoloff, D. D. & Kuzanyan, K. 2010, *MNRAS*, 402, L30.